Supporting Information

Glauser et al. 10.1073/pnas.1116712108

SI Materials and Methods

Below we present our *Combinatorial Alternate Exon quantitative PCR* (CAE-qPCR) method and its validation and provide full experimental procedures for analysis of wild-type and mutant *Caenorhabditis elegans* strains.

CAE-qPCR Method. We used a probe hydrolysis-based (Taqman) strategy to quantify the expression of the 12 *slo-1* splice variants because it relies on specific hybridization of oligonucleotides at three sites along the target cDNA. Our method uses primer pairs that specifically hybridize to the 5′ alternate exon (A1 or A2) and the 3′ alternate exon (C0 or C1) of the target cDNA and probes that hybridize to a specific alternate exon at site B (B0, B1, or B2) (Fig. 2*A*). Each probe has a fluorophore and a quencher covalently bound to the 5′ end and the 3′ end, respectively. At each PCR cycle, the endonuclease 5′–3′ activity of Taq polymerase cleaves the probe, releasing the fluorophore from the quencher and allowing real-time monitoring of target amplification. Using the set of primers and probes with high binding specificities, each of the 12 A-B-C primer and probe combinations should detect only one single transcript. Below we describe our strategy for optimizing primer and probe sets to specifically amplify target transcripts with minimal cross-reactivity to other splice variants. This validation process leveraged the set of plasmids carrying full-length *slo-1* splice variants used in our biophysical characterization of the properties of alternative BK channel isoforms (1).

Primer validation. We designed primers (Fig. S1*A* and Table S1) that specifically hybridize to each alternate exon with minimal cross-reactivity. To quantify the expression of transcripts lacking inserts at sites B and C, we designed primers that span the splice junction between the flanking constitutive exons. To validate that the selected primers could efficiently amplify the target transcripts when present in a complex template mixture, we evaluated their ability to amplify *slo-1* transcripts in a *C. elegans* cDNA library generated by reverse transcription (RT) of total RNA with random hexamers. PCR reactions were performed with each of the four A/C primer pairs, followed by electrophoresis analysis. The four reactions produced bands of expected size (500–550 bp) (Fig. S1*B*). The products were cleaved by *Bsm*I restriction enzyme digestion, and the fragments were of the predicted sizes (Fig. S1*B*), confirming the specific amplification of *slo-1*. Slight differences in size allowed a gross evaluation of B site splicing events using PCR products obtained from cDNA plasmid templates as a size standard.

Next, we used a dye-based real-time qPCR approach to further optimize cycling parameters and to quantitatively evaluate the cross-reactivity of each A-C primer pair with the nontargeted splice variants. Each primer pair was tested against four cDNA plasmid templates (in each case, one match and three mismatch templates). Representative amplification profiles are shown in Fig. S1*C*. For A1/C0, A1/C1, and A2/C1 primer pairs, a shift of at least 10 cycles was observed between match and mismatch templates. This indicates that the signal generated for targeted splice variants is at least three orders of magnitudes (2^{10}) higher than the one generated with nonspecific templates, assuming ideal amplification efficiency. The A2/C0 primer pair did amplify a nonspecific A1;C0-type splice variant with ≈100-fold (2^7) lower efficiency than the target splice variant. Cross-reactivity will therefore be negligible in samples in which all variants are present in similar abundance. However, for transcripts expressed at relatively low levels, a significant fraction of the signal may be due to cross-reactivity with nonspecific templates present at much higher concentration. To quantitatively evaluate this effect, we calculated a cross-reactivity factor for each mismatched combination of templates and primer pairs (Tables S2 and S3). These factors were used to control a posteriori for cross-reactivity in the data obtained with RT-derived cDNA templates.

Probe validation. We designed hydrolysis probes to specifically recognize each of the three possible splicing events at site B: B0, B1, or B2. Although the probe targeted to B2 complements a unique sequence that is missing from B1 and B0 variants, probes targeted to B0 and B1 hybridize to exon boundaries where portions of the hybridizing sequence is shared by multiple splice variants, presenting a risk for cross-reactivity. We evaluated this risk by performing real-time PCR analysis with plasmid cDNA templates. Each probe was tested against three cDNA templates (in each case, one match and two mismatch templates; Fig. S1*D*). The match templates all gave stronger signals, which were detectable at lower cycles than the mismatch templates. Cross-reactivity factors were calculated for each probe on the basis of the cycle differences (Tables S2 and S3). Because this factor is strongly dependent upon the set signal threshold for quantitative cycle determination, we held the signal threshold constant for all CAE-qPCR measurements.

qPCR efficiency. The amplified portion of each *slo-1* splice variant is longer than the 150- to 200-base pair amplicons typically recommended for efficient probe-hydrolysis qPCR. We sought to control for this empirical limitation by measuring the efficiency and accuracy of the probe-hydrolysis qPCR for detecting each of the 12 splice variants. To do this, we used probe-hydrolysis qPCR to amplify plasmid cDNAs and to generate standard curves covering three orders of magnitude in copy number variation (10–10,000). The cycle where the fluorescence signal crossed the threshold (C_t) was plotted as a function of the logarithm of the initial template concentration. The best linear fit was calculated by linear regression. Table S4 reports the thresholds, slopes, intercepts, regression coefficients (R^2), and the calculated PCR efficiencies. R^2 values were above 0.99, and the calculated efficiency average was 97% (SD 6%), indicating that the large amplicon size limited neither signal detection nor amplification.

Controlling for cross-hybridization effects in worm lysate-derived cDNA samples. With the CAE-qPCR method in place, we quantified the absolute abundance of each of the 12 *slo-1* splice variants from worm lysate-derived cDNA samples. To begin, we prepared total RNA samples from five independent populations of young adult wild-type (N2) animals. Next, samples were reverse transcribed with a *slo-1*–specific primer that hybridized to the boundary between the constitutive exons 17 and 18, downstream of the alternatively spliced region of the gene. Finally, we used CAE-qPCR to measure splice variant expression. We converted C_t values to copy number using the standard curves generated from plasmid cDNA templates, yielding an absolute quantification of splice variant copy number. Between 10 and 4,300 copies were detected per CAE-qPCR reaction. It was therefore important to carefully evaluate cross-hybridization of primers and probes to avoid overestimating the amount of the least abundant transcripts. Cross-reactivity factors previously determined for each probe and primer combination (Tables S2 and S3) were used to calculate the fraction of the measured copy number that was caused by amplification and detection of nonspecific templates. For 10 of the 12 splice variants, the maximum error due to cross-reactivity was significantly smaller than the SD of the measured values across five replicates. The remaining two splice variants

A1;B0;C0 and A1;B0;C1 produced very low amplification signals, and the calculated cross-reactivity errors were similar to the measured signal. Thus, these two transcripts were expressed below the detection threshold and were omitted from further analyses.

Controlling for PCR reagent titration in multitemplate samples. PCR reagent-titration effects bias the results of quantitative PCR analysis when the DNA template contains a mix of splice variants present at very different concentrations (2). These effects occur among splice-variant amplicons that have identical primer-hybrization sequences but contain distinct probe-binding sites. For *slo-1* splice variants analyzed by CAE-qPCR, three templates are amplified in parallel by each A/C primer pair (one containing B0, one containing B1, and one containing B2) regardless of the probe used to monitor the reaction. Thus, competition effects may produce a titration of PCR reagents during the amplification of nontargeted splice variants. The amplification of the least abundant transcript produces a weaker signal, likely owing to the depletion of primers and/or the saturation of the polymerase by the parallel amplification of more abundant, nontargeted splice variants.

To determine whether significant underestimations arose from such competition effects, we empirically measured the concentration ratio at which a competing nontargeted splice variant affects amplification efficiency for the targeted splice variant. Among A2;C0-type splice variants there is a ≈20-fold difference in expression levels, so we evaluated how the presence of the abundantly expressed A2;B0;C0 splice variant affected the detection of the less-abundant transcript A2;B1;C0. Fig. S2*A* compares amplification profiles obtained from pure plasmid cDNA and mixed-template RT-derived cDNA samples for both A2;B0;C0 and A2;B1;C0. qPCR amplification curves for reactions containing a single template of either A2;B0;C0 or A2;B1;C0 show strong signals with a large range of exponential amplification (linear portion of the curve in the semilog plot, Fig. S2*A*). The amplification profile for A2;B0;C0 from RT-derived template cDNA is similar to that of pure plasmid cDNA, indicating that this abundant transcript is, as expected, not subject to a competition effect. In the case of A2;B1;C0, amplification traces obtained from RT-derived cDNA samples reached lower signal amplitude than the signal obtained with pure plasmid templates. These observations suggest that the shift is likely due to a competition effect.

Generally, the signal intensity threshold for measuring C_t is set in the middle of the exponential range of the fluorescence curve, where the signal to noise ratio is high. For splice variants expressed at low levels, the exponential range of the fluorescent signal was often very narrow. We minimized the effects of PCR reagent titration by finding the minimum usable signal threshold that would not compromise the signal to noise ratio or the measured amplification efficiency. To establish this optimal signal threshold, pure cDNA templates of A2;B0;C0 and A2;B1;C0 of known concentration were mixed to recreate the conditions from the worm cDNA template pool. First, the A2;B1;C0 target cDNA was held constant while the amount of A2;B0;C0 competitor cDNA was progressively increased. Increasing the competitor cDNA decreased the amplitude of signal but not the C_t value when the threshold was set below 0.01 (Fig. S2*B*).

To evaluate the concentration difference between target and competing splice variants at which the PCR reagent titration effect would bias the analysis, we compared standard curves for the A2;B1;C0 target generated in the presence or absence of the A2;B0;C0 competitor. We used the same concentration of A2;B0;C0 as was measured from the mixed worm cDNA pool generated by RT. The fluorescence profile of the A2;B1;C0 splice variant in the presence of competitor deviates from the control reaction (with no competitor) when the competing A2;B0;C0 splice variant concentration is 25-fold more abundant than the target splice variant (Fig. S2*C*). This result suggests that the PCR reagent titration effect did not cause a significant bias in the quantification of A2;B1;C0, because the maximum difference in RT-derived cDNA samples was 20-fold. To further confirm this conclusion, we created a plasmid cDNA mix that recapitulated the measured values and compared these results with those obtained from the worm cDNA pool. The amplification profiles were very similar, recapitulating the decreased signal amplitude at high cycles and yielding the same C_t at the established signal threshold (Fig. S2*D*). Thus, PCR reagent titration effects can be minimized by empirically determining the signal threshold value at which the results from both pure cDNA and mixed RT-derived cDNA templates are congruent.

Collectively, the results of our detailed analysis of cross-reactivity and titration effects indicate that the CAE-qPCR method developed here produced an accurate and absolute quantification of *slo-1* splice variants.

Primer Design and Synthesis. Exon-specific primers were used in the CAE-qPCR technique and for dye-based qPCR. Although the A1 and A2 alternate exons are similar in sequence, we designed primers that hybridize with unique regions in each alternate exon. C1 primer design was straightforward because it recognizes a sequence that is only present in C1-type variants. The C0 splicing event is the exclusion of exon 15 and the introduction of a junction between exon 14 and 16 that is absent from C1-type variants. Four candidate primers overlapping this exon boundary were tested by standard PCR with plasmid templates carrying cDNA clones for C0 and C1 variants. One of the primers, showing no detectable cross-reactivity with C1 containing templates, was selected. Additional primers were used to quantify the abundance of all *slo-1* transcripts (forward primer at the boundary of exons 16 and 17, reverse primer on exon 18), as well as the abundance of reference genes by dye-based qPCR. All primers were synthesized at the Protein and Nucleic Acid Facility at Stanford University. Sequences are reported in Table S1.

Probe Design and Synthesis. We designed hydrolysis probes (Taqman probes) to recognize each of the three possible splicing events at site B: B0, B1, or B2. For the B2-specific probe, we targeted the unique sequence at the 5′ end of exon 13 that is missing from B1 and B0 variants. For the B1-specific probe, we targeted the boundary between exon 12 and the B1 form of exon 13. This is the only region that differs from B2 variants. For the B0 specific probe, we targeted the boundary between exon 12 and 14. Two candidate B0 probes were tested; we selected the one with the least cross-reactivity with B1 and B2. All probes were covalently bonded to Fam fluorophore in 5′ and a black hole quencher (BHQ) in 3′ and were synthesized at Biosearch Technologies. Probe sequences are reported in Table S1.

Quantitative PCR. Dye-based qPCR experiments were performed with PowerSYBR Master Mix (Applied Biosystems) in a final volume of 20 μL. We evaluated total cDNA abundance from RT-derived samples for wild-type (N2) and *slo-1*(*pg52*) animals by quantifying the expression of two reference genes, *cdc-42* and *pmp-3*, whose expression was previously shown to be very stable (3). For the CAE-qPCR approach, probe hydrolysis (Taqman) analyses were performed with Taqman Gene Expression Master Mix (Applied Biosystems) in a final volume of 30 μL. Primer and probe final concentrations were 1 μM and 500 nM, respectively. All real-time PCR experiments were performed in a StepOnePlus apparatus (Applied Biosystems) at the Protein and Nucleic Acid Facility at Stanford University. The default thermal cycling profile was used, except for the elongation time, which was extended to 30 s, and the annealing temperature, which was increased to 63 °C. These parameters minimized cross-reactivity between splice variants, without impairing PCR efficiency.

Standard curves for absolute quantification were made with serial dilutions of plasmids carrying each of the 12 *slo-1* splice variants and were included in each PCR run. Control reactions lacking reverse transcriptase ("*No reverse transcriptase*") and cDNA templates ("*No cDNA template*") were analyzed in parallel. For dye-based qPCR experiments, dissociation curves were performed to verify that a unique product was amplified for both plasmid cDNA and RT-derived sample cDNA templates. For RT-derived samples, cDNA templates generated from 40 ng of starting total RNA were analyzed in each reaction. Results are reported as cDNA copy numbers in a sample of this size.

Sequencing. To identify the *pg52* point mutation, genomic DNA was amplified using standard PCR conditions (see primer sequences in Table S1) and sequenced (Sequetech).

***C. elegans* Strain Maintenance, Total RNA Extraction, and RT.** *C. elegans* nematodes were maintained and age-synchronized according to standard procedures (4). We used homogenous, synchronized populations of young adult animals for behavioral analysis, RNA extraction, and RT. Total RNA was extracted with TRIzol reagent (Invitrogen), and five independent replicates were analyzed for each genotype. RNA (12 μg) from each sample was reverse transcribed with the SuperScript Vilo cDNA Synthesis Kit (Invitrogen) in a final volume of 100 μL according to supplier instructions, except that 10 μM of the *slo-1* variable region-specific reverse primer CCACGTGTTTGAGCTCATGAT was included in the reaction mix in addition to random hexamers. All samples and controls were purified and concentrated (Zymo Research) to a final volume of 100 μL.

***C. elegans* Chemical Mutagenesis, Genetic Screen, and Behavioral Studies.** Synchronized (L4-stage) *unc-2(ra612)* animals were mutagenized by exposure to ethyl methanesulfone (EMS) according to standard procedures (5). Briefly, animals were washed off growth plates, pelleted, resuspended in M9 saline (4 mL) containing EMS (225 μM), and incubated with gentle agitation for 4 h. Next, animals were washed twice in fresh M9 and transferred to growth plates seeded with OP50 *Escherichia coli* for 1–2 h. Twenty healthy, young adult P0 animals were transferred to individual plates and incubated at 20 °C for 24 h. P0s were removed from the plates, and F1s were incubated for another 48 h. Five hundred F1 animals were transferred to individual growth plates; their F2 progeny were assayed for sensitivity to aldicarb when most animals in each population were at the young adult stage.

Aldicarb hypersensitive individuals were selected and used to establish lines of putative mutants, which were tested in subsequent generations to identify true-breeding mutants and eliminate false positives. We assayed sensitivity to aldicarb as follows. First, F2 populations were transferred to small (35 mM) nematode growth medium (NGM) agar assay plates containing aldicarb (1 mM; Chem Service) for 3 h. Next, the degree of paralysis observed in F2 animals was compared with control *unc-2(ra612)* animals, which are resistant to aldicarb-induced paralysis. Finally, we selected individual paralyzed animals (putative mutants) and transferred them to individual growth plates. Aldicarb hypersensitivity was confirmed in the F3 and F4 generations. For both genetic screening and behavioral studies, aldicarb assay plates were prepared by pouring 3 mL molten NGM agar containing aldicarb (1 mM) into small Petri plates (35 mm). Plates were used within 2 d.

We measured aldicarb sensitivity of wild-type and mutant animals as follows. Between 20 and 25 animals were placed onto aldicarb plates, and the number of paralyzed worms was counted every 30 min for the duration of the assay. We defined a paralyzed animal as one that is unable to move any part of its body during a 2- to 3-s observation period. Animals were not stimulated to determine paralysis. Data presented in Fig. 3*B* were obtained with Worm Tracker (6), providing a semiautomated quantification of the paralysis kinetics.

Probability-Based Modeling. Nonconditional probabilities were calculated from the frequency of each splice variant in the total pool of *slo-1* transcripts. Conditional probabilities were calculated from the frequency of each variant in subgroups as follows:

$P(A_i|B_j)$ = P(all A_i;B_j containing variants)/P(all B_j containing variants)
$P(B_j|A_i)$ = P(all A_i;B_j containing variants)/P(all A_i containing variants)
$P(A_i|C_k)$ = P(all A_i;C_k containing variants)/P(all C_k containing variants)
$P(C_k|A_i)$ = P(all A_i;C_k containing variants)/P(all A_i containing variants)
$P(B_j|C_k)$ = P(all B_j;C_k containing variants)/P(all C_k containing variants)
$P(C_k|B_j)$ = P(all B_j;C_k containing variants)/P(all B_j containing variants)
$P(A_i|B_j;C_k)$ = $P(A_i;B_j;C_k$ containing variants)/P(all $B_j;C_k$ containing variants)
$P(B_j|A_i;C_k)$ = $P(A_i;B_j;C_k$ containing variants)/P(all $A_i;C_k$ containing variants)
$P(C_k|A_i;B_j)$ = $P(A_i;B_j;C_k$ containing variants)/P(all $A_i;B_j$ containing variants),

where i is 1 or 2, j is 0, 1 or 2, and k is 0 or 1.

For example, the probability of B1 knowing the occurrence of A1 was calculated as follows:

P(B1|A1) = P(all A1;B1 containing variants)/P(all A1 containing variants).

In each model, the predicted probability of a specific variant was calculated by multiplying the probability (conditional or nonconditional) of exon choices at the three sites. The predicted copy number of a given variant was obtained by multiplying the total measured copy number of *slo-1* transcripts by the predicted probability of a specific variant.

1. Johnson BE, et al. (2011) Alternatively spliced domains interact to regulate BK potassium channel gating. *Proc Natl Acad Sci USA*, 10.1073/pnas.1116795108.
2. Vandenbroucke II, Vandesompele J, Paepe AD, Messiaen L (2001) Quantification of splice variants using real-time PCR. *Nucleic Acids Res* 29:E68.
3. Hoogewijs D, Houthoofd K, Matthijssens F, Vandesompele J, Vanfleteren JR (2008) Selection and validation of a set of reliable reference genes for quantitative sod gene expression analysis in *C. elegans*. *BMC Mol Biol* 9:9.
4. Stiernagle T (2006) Maintenance of C. elegans. *WormBook* Feb 11:1–11.
5. Jorgensen EM, Mango SE (2002) The art and design of genetic screens: *Caenorhabditis elegans*. *Nat Rev Genet* 3:356–369.
6. Ramot D, Johnson BE, Berry TL Jr., Carnell L, Goodman MB (2008) The Parallel Worm Tracker: A platform for measuring average speed and drug-induced paralysis in nematodes. *PLoS ONE* 3:e2208.

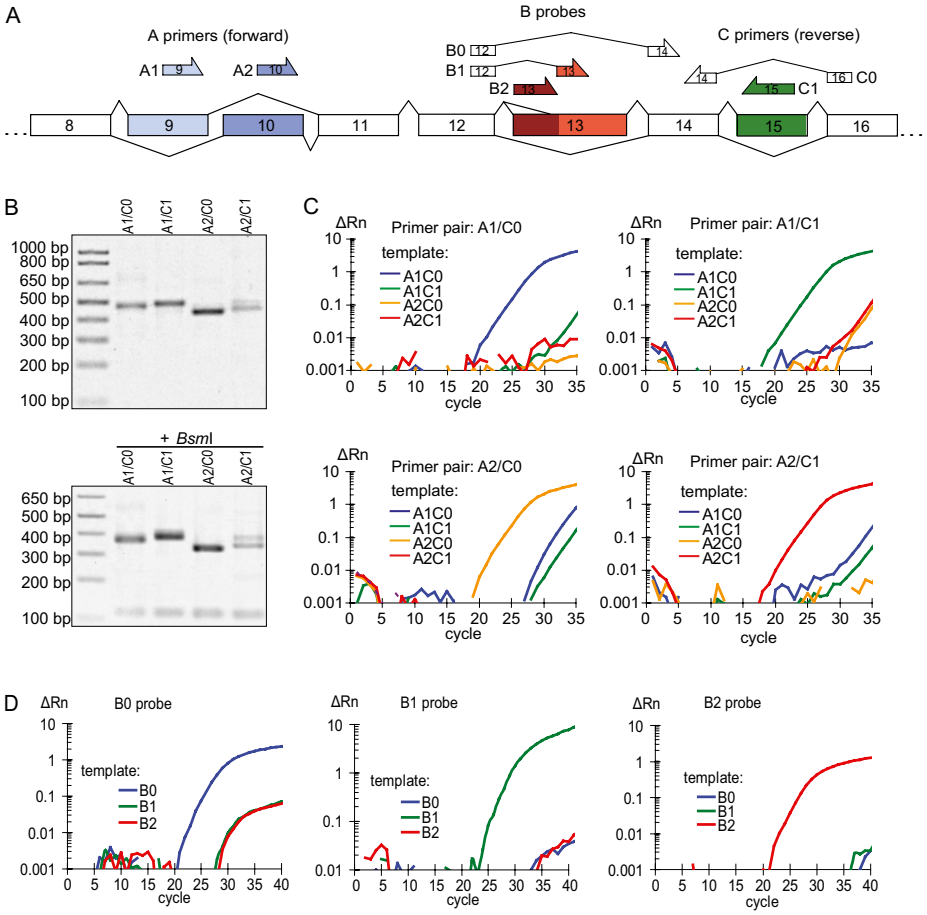

Fig. S1. CAEq-PCR method. (*A*) Schematic of the alternatively spliced region of *slo-1* and primer and probe recognition sequences. (*B*) Qualitative analysis of PCR products for each A/C primer pair. The template was a cDNA library generated by RT with random hexamers and a *slo-1* gene-specific primer from total adult worm RNA extracts. PCR products were digested with *BsmI* where indicated, yielding fragments of the expected size for *slo-1* specific amplification. (*C*) The specificity of each A/C primer pair was assessed by real-time PCR analysis (SYBR green). Each panel depicts representative amplification curves for the indicated A/C primer pair. In each case, separate reactions were run with four plasmid templates carrying the indicated *slo*-1 splice variants (one match, three mismatches). ΔR_n, relative fluorescence changes after baseline subtraction. (*D*) The specificity of each B probe was assessed by probe-hydrolysis (Taqman) qPCR with matched A/C primers. Each panel depicts representative amplification curves for the indicated probe. In each case, separate reactions were run with three plasmid templates carrying the indicated *slo-1* splice variants (one probe match, two probe mismatches). ΔRn, relative fluorescence changes after baseline subtraction.

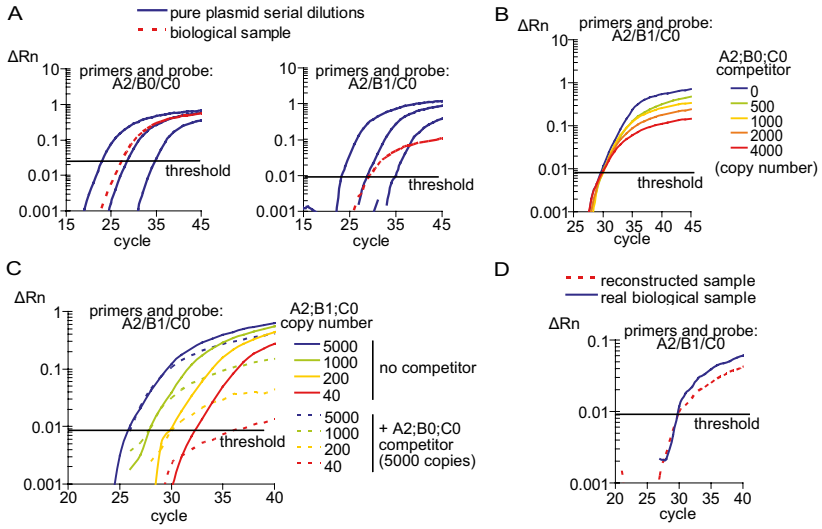

Fig. S2. Analysis of the titration effect in CAE-qPCR between A2;B1;C0 (target) and A2;B0;C0 (competitor). (*A*) Representative A2;B0;C0 and A2;B1;C0 amplification curves are depicted for pure plasmid serial dilutions and worm lysate-derived cDNAs (biological sample). Copy numbers for pure plasmids were 30,000, 1,200, and 48 for A2;B0;C0; and 6,250, 250, and 10 for A2;B1;C0. (*B*) 250 copies of A2;B1;C0 were amplified in the presence of the indicated copy numbers of the A2;B0;C0 competitor (both templates from plasmid). Reactions were performed in triplicate with the A2/B1/C0 primer and probe set. Representative amplification curves are depicted. (*C*) Indicated numbers of A2;B1;C0 copies were amplified in the absence or presence of 5,000 copies of A2;B0;C0 competitor (both templates from plasmids). Reactions were performed in triplicate with the A2/B1/C0 primer and probe set. Representative amplification curves are depicted. (*D*) A mix of A2;B0;C0 and A2;B1;C0 plasmid cDNAs was made to match the concentration measured in worm lysate-derived cDNAs. This reconstructed sample was compared with worm lysate-derived cDNAs (real biological sample). Reactions were performed in triplicate with the A2/B1/C0 primer and probe set. Representative amplification curves are depicted. ΔRn, relative fluorescence changes after baseline subtraction.

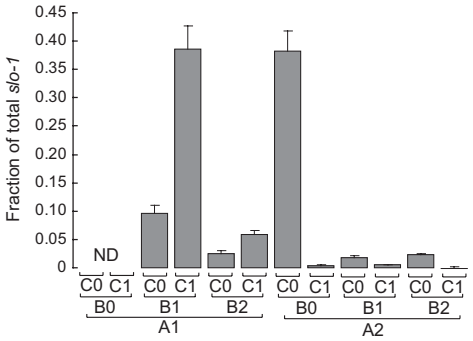

Fig. S3. Measured distribution of the 12 *slo-1* variants in wild type. Copy numbers of each *slo-1* splice variant were measured by CAE-qPCR, and the fraction of the total copy number is shown for each splice variant. Errors bars are 99% confidence intervals of the means. ND, not detectable.

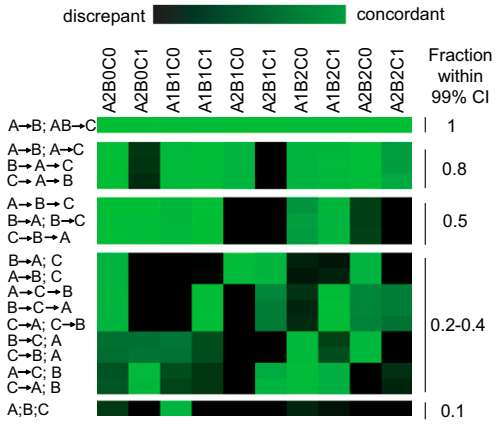

Fig. S4. Systematic survey of conditional probability models. Models assuming zero, one, or two interactions among splicing decisions at sites A, B, and C were created as described in *SI Materials and Methods*. Predicted values were calculated for wild type and compared with measured values. Models were clustered according to the fraction of splice variants for which predictions were within the 99% confidence interval of the mean measured values. Data were log transformed, and the differences between predicted and empirical values were used to create a color scale reflecting the level of concordance/discrepancy between them. In the model description, arrows indicate interactions, and semicolons separate independent splicing decisions.

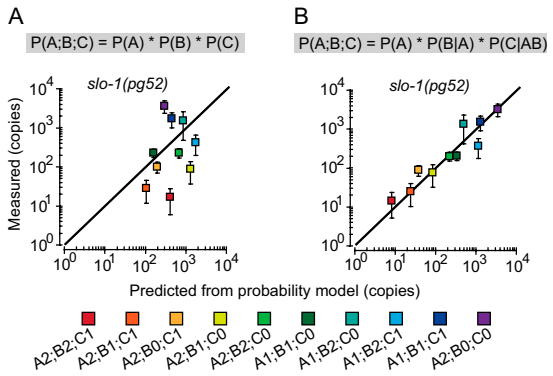

Fig. S5. Probability-based modeling for the *pg52* mutant. Copy numbers of each *slo-1* splice variant were measured by CAE-qPCR in *pg52* adult worms and their means plotted against the corresponding predicted values. (*A* and *B*) Predictions were calculated according to the indicated formulas. Error bars are 99% confidence intervals of the means ($n = 5$). The solid line shows the relationship expected for a perfect match between the two datasets. Probability values for the independent splicing model (*A*) were: $P(A1) = 0.349$, $P(A2) = 0.651$, $P(B0) = 0.449$, $P(B1) = 0.220$, $P(B2) = 0.331$, $P(C0) = 0.810$, and $P(C1) = 0.190$. Probability values for the interdependent splicing model (*B*) were: $P(A1) = 0.349$, $P(A2) = 0.651$, $P(B0|A1) = 0.000$, $P(B1|A1) = 0.498$, $P(B2|A1) = 0.502$, $P(B0|A2) = 0.912$, $P(B1|A2) = 0.028$, $P(B2|A2) = 0.060$. $P(C0|A1B0) = 0.000$, $P(C1|A1B0) = 0.000$, $P(C0|A1B1) = 0.118$, $P(C1|A1B1) = 0.882$, $P(C0|A1B2) = 0.785$, $P(C1|A1B2) = 0.215$, $P(C0|A2B0) = 0.973$, $P(C1|A2B0) = 0.027$, $P(C0|A2B1) = 0.754$, $P(C1|A2B1) = 0.246$, $P(C0|A2B2) = 0.933$, and $P(C1|A2B2) = 0.067$.

Table S1. Oligonucleotide sequences

Name	Sequence (5′ to 3′)	Use
slo-1 A1 fwd	GAGTCCTTCGTTTGCGAATATGTCA	CAE-qPCR
slo-1 A2 fwd	ATCCCACTCGTTCGTCGGAA	CAE-qPCR
slo-1 C0 rev	CGGAAGATGGCCTCTGTTGA	CAE-qPCR
slo-1 C1 rev	GTGTTGAGATGAGTATCACTCG	CAE-qPCR
slo-1 B0 probe	GGCCCGTGCAAGAGCCACCGA	CAE-qPCR
slo-1 B1 probe	CCCGTGATTATTCGGACTTTGAC	CAE-qPCR
slo-1 B2 probe	CGGCCCGTGAAAAAAATGCCAA	CAE-qPCR
total *slo-1* fwd	TTGAGCAGCAATTCCAAGACATGAA	Dye-based qPCR
total *slo-1* rev	GCGCGTAAATCTGCTCGAGATAG	Dye-based qPCR
cdc-42 fwd	CTGCTGGACAGGAAGATTACG	Dye-based qPCR
cdc-42 rev	CTCGGACATTCTCGAATGAAG	Dye-based qPCR
pmp-3 fwd	GTTCCCGTGTTCATCACTCAT	Dye-based qPCR
pmp-3 rev	ACACCGTCGAGAAGCTGTAGA	Dye-based qPCR
*slo-1*A1 fwd	GAGTCCTTCGTTTGCGAATATGTCA	Dye-based qPCR at site A
*slo-1*A2 fwd	ATCCCACTCGTTCGTCGGAA	Dye-based qPCR at site A
slo-1 A rev	GAAACGTCCTTAATATCGTCATGACACT	Dye-based qPCR at site A
slo-1 B fwd	GCTTCTTCTTCTGGCGATTGAGC	Dye-based qPCR at site B
slo-1 B0 rev	TGGCTCTTGCACGGGC	Dye-based qPCR at site B
slo-1 B1 rev	CGTCAAAGTCCGAATAATCACGGG	Dye-based qPCR at site B
slo-1 B2 rev	CGAATAATCTGAAATTTTGGCATTTTTTTCACG	Dye-based qPCR at site B
slo-1 C fwd	AGTGTCATGACGATATTAAGGACGTTTC	Dye-based qPCR at site C
slo-1 C0 rev	CGGAAGATGGCCTCTGTTGA	Dye-based qPCR at site C
slo-1 C1 rev	GTGTTGAGATGAGTATCACTCG	Dye-based qPCR at site C
slo-1 exon 1 fwd	CCACTAGTTTCTGGTGATGAC	*slo-1* sequencing
slo-1 exon 1 rev	TTGAAAGCTGGCAACCTCAG	*slo-1* sequencing
slo-1 exon 2 fwd	GCTCTCACTCTTCCAAATCC	*slo-1* sequencing
slo-1 exon 2 rev	AGCTGCATCGCTAGAGAATC	*slo-1* sequencing
slo-1 exon 3 fwd	ACCGAGTGAGTTTGATGTAGC	*slo-1* sequencing
slo-1 exon 5 rev	CATATCAGCTGGGTTCTGAG	*slo-1* sequencing
slo-1 exon 6 fwd	CTCAGAACCCAGCTGATATG	*slo-1* sequencing
slo-1 exon 6 rev	GTCGGCCGCAAAGCGTCGTAC	*slo-1* sequencing
slo-1 exon 7 fwd	GTAAAACTGTCCTGTGTACC	*slo-1* sequencing
slo-1 exon 7 rev	AGTCGCATAACTCAGTCAG	*slo-1* sequencing
slo-1 exon 8 fwd	GAGATCCATATCTCAGGCAG	*slo-1* sequencing
slo-1 exon 8 rev	ATGATGTCCCATGTGCATGC	*slo-1* sequencing
slo-1 exon 9 fwd	CGAAAGTAGGCCGTTTCAG	*slo-1* sequencing
slo-1 exon 9 rev	CCTATCTTGGCATGGTTTG	*slo-1* sequencing
slo-1 exon 10 fwd	ATTTCTGGCCCAAATTAGGC	*slo-1* sequencing
slo-1 exon 10 rev	TGTTCGATTCACCTTGTCGA	*slo-1* sequencing
slo-1 exon 11 fwd	TTGGACATGCTAGATCGAC	*slo-1* sequencing
slo-1 exon 11 rev	GATTATGGTCGATATGGGTG	*slo-1* sequencing
slo-1 exon 12 fwd	CCTAGTCAATATGGATGTCATACG	*slo-1* sequencing
slo-1 exon 13 rev	AAACAGAGCGTCAAAGTCC	*slo-1* sequencing
slo-1 exon 14 fwd	TATAGCGAATATGGGTGTC	*slo-1* sequencing
slo-1 exon 15 rev	TTCAAAGGCGTCTAAGGGTGTG	*slo-1* sequencing
slo-1 exon 16 fwd	GCTCACTTTTCAGCTTTCTAGC	*slo-1* sequencing
slo-1 exon 16 rev	CAGAAGCTGAAAACTTGCTTG	*slo-1* sequencing
slo-1 exon 17 fwd	GAGTTTTCGCAGTAAGACC	*slo-1* sequencing
slo-1 exon 17 rev	CCATAACTTTGTTCAATCTCAACG	*slo-1* sequencing
slo-1 exon 18 fwd	GGTTCCAAAATAGTGTTTCTTGACC	*slo-1* sequencing
slo-1 exon 18 rev	TGTTCGAACCCACCAAGCTC	*slo-1* sequencing
slo-1 exon 19 fwd	GTCGCAGTATTATTTCAAGC	*slo-1* sequencing
slo-1 exon 19 rev	GTCGCGTAACTTTGTCAG	*slo-1* sequencing
slo-1 exon 20 fwd	CGAAATAGGCCGATAAGC	*slo-1* sequencing
slo-1 exon 20 rev	CGGTACACTGCAGCTTAAAACTGG	*slo-1* sequencing
slo-1 exon 21 fwd	CCTAGCCAATATGAGTGTC	*slo-1* sequencing
slo-1 exon 22 rev	ATTCAGGTCCACACGATACC	*slo-1* sequencing

Table S2. Cross-reactivity factors for B-type exons

	B-type exon in template		
Probe	B0	B1	B2
B0	—	0.031	0.025
B1	ND	—	ND
B2	ND	ND	—

ND, not detected (<0.001).

Table S3. Cross-reactivity factors for A/C exon combinations

	AC combination in template			
Primer pair	A1C0	A1C1	A2C0	A2C1
A1/C0	—	ND	ND	ND
A1/C1	ND	—	ND	0.004
A2/C0	0.006	ND	—	ND
A2/C1	ND	ND	ND	—

ND, not detected (<0.001).

Table S4. CAE-qPCR standard curve values

Variant	Threshold	Slope	Intercept	R^2	Calculated efficiency (%)
A1B0C0	0.005	−3.23	27.86	0.996	104
A1B0C1	0.006	−3.89	28.24	0.991	81
A2B0C0	0.028	−3.32	30.14	0.999	100
A2B0C1	0.029	−3.35	30.12	0.999	99
A1B1C0	0.034	−3.32	29.20	0.998	100
A1B1C1	0.016	−3.31	28.13	0.996	100
A2B1C0	0.009	−3.33	28.21	0.988	100
A2B1C1	0.011	−3.37	27.55	0.995	98
A1B2C0	0.034	−3.47	29.32	0.997	94
A1B2C1	0.031	−3.43	28.96	0.999	96
A2B2C0	0.039	−3.49	29.16	0.992	94
A2B2C1	0.019	−3.40	28.06	0.999	97

Table S5. Predicted vs. measured copy numbers of *slo-1* variants in wild type

	slo-1 variants											
Predicted values according to model:	A1B0C0	A1B0C1	A2B0C0	A2B0C1	A1B1C0	A1B1C1	A2B1C0	A2B1C1	A1B2C0	A1B2C1	A2B2C0	A2B2C1
A;B;C	1,666	625	1,964	737	**1,363**	511	1,606	603	683	256	805	302
A->B;C	0	0	3,097	1,162	3,903	1,465	**192**	**72**	709	266	**186**	70
A;B->C	1,976	21	2,330	**26**	605	1,958	714	2,309	**241**	302	**284**	356
A->C;B	633	2,215	2,095	**51**	517	1,811	1,713	**42**	**259**	907	858	21
B->A;C	0	0	3,165	1,188	3,862	1,449	**200**	**75**	674	253	**186**	70
C->B; A	1,962	2,056	2,313	2,424	590	128	696	151	**245**	124	**288**	146
C->A;B	611	2,204	2,125	**54**	499	1,802	1,738	**44**	**250**	903	871	22
A->B; A->C	0	0	**4,157**	102	**1,193**	**4,175**	**258**	6	**217**	**758**	**250**	**6**
A->B->C	0	0	**4,213**	**46**	**1,267**	**4,100**	62	202	433	**543**	114	143
A->C->B	989	4,396	**3,273**	102	297	273	985	6	123	264	408	**6**
B->A; B->C	0	0	**4,306**	**47**	**1,254**	**4,057**	65	210	411	**516**	114	143
B->A->C	0	0	**4,249**	104	**1,180**	**4,130**	**269**	7	**206**	**721**	**250**	**6**
B->C->A	961	46	**3,345**	1	294	**4,166**	1,024	101	117	**643**	408	16
C->A;C->B	954	4,374	**3,321**	106	287	272	999	7	119	263	414	**6**
C->A->B	0	0	**4,219**	106	**1,151**	**4,154**	**262**	7	**209**	**755**	**254**	**6**
C->B->A	0	0	**4,276**	4,480	**1,223**	265	63	14	418	211	115	58
A->B; AB->C	0	0	**4,334**	**47**	**1,149**	**4,372**	**211**	**61**	**301**	**702**	**254**	**9**
Measured values (mean)	ND	ND	4,249	46	1,071	4,296	207	60	280	655	249	9
99% CI lower bound	ND	ND	3,205	26	649	3,131	115	41	158	433	177	5.7
99% CI upper bound	ND	ND	5,292	67	1,492	5,461	299	79	402	877	321	12.4

Predicted values that are within the 99% confidence interval (CI) of the measured values are in bold.

Table S6. Predicted vs. measured copy numbers of *slo-1* variants in *pg52* mutant

	slo-1 variants											
Predicted values according to model:	A1B0C0	A1B0C1	A2B0C0	A2B0C1	A1B1C0	A1B1C1	A2B1C0	A2B1C1	A1B2C0	A1B2C1	A2B2C0	A2B2C1
A;B;C	949	223	1,768	415	464	109	864	203	**699**	164	1,303	306
A->B;C	0	0	**3,589**	842	1,053	247	**110**	**26**	**1,059**	**249**	**235**	55
A;B->C	1,141	31	2,125	58	88	485	164	903	**692**	171	1,290	319
A->C;B	530	641	2,106	**77**	**259**	313	1,029	**38**	391	**473**	1,552	57
B->A;C	0	0	**2,717**	638	1,254	294	**74**	**17**	**1,780**	**418**	**222**	52
C->B; A	1,342	22	**2,501**	40	117	379	218	706	**653**	95	1,217	177
C->A;B	841	597	1,876	40	411	292	917	**20**	**620**	**440**	1,383	30
A->B; A->C	0	0	**4,276**	156	588	712	132	5	**592**	716	280	10
A->B->C	0	0	**4,314**	**118**	**199**	**1,101**	21	115	**1,049**	**259**	**233**	58
A->C->B	750	62	**2,979**	7	65	**1,092**	259	131	365	**273**	1,449	33
B->A; B->C	0	0	**3,266**	**89**	**237**	**1,311**	14	77	**1,762**	**436**	**220**	54
B->A->C	0	0	**3,237**	**118**	701	847	**88**	3	**995**	1,203	**265**	**10**
B->C->A	1,011	84	**2,255**	6	78	**1,301**	174	88	**613**	**459**	1,369	31
C->A;C->B	1,189	58	**2,654**	4	104	**1,017**	231	69	**579**	**255**	1,291	**17**
C->A->B	0	0	**3,809**	**82**	933	663	**117**	3	**939**	667	**250**	**5**
C->B->A	0	0	**3,843**	62	316	**1,025**	19	60	**1,662**	**242**	**207**	30
A->B; AB->C	0	0	**3,575**	39	349	**1,326**	**86**	**25**	**505**	1,180	**228**	**8**
Measured values (mean)	ND	ND	3,391	93	214	1,604	81	26	1,437	393	213	15
99% CI lower bound	ND	ND	2,221	64	163	944	34	11	445	185	158	5
99% CI upper bound	ND	ND	4,561	121	266	2,263	128	42	2,429	600	268	25

Predicted values that are within the 99% confidence interval (CI) of the measured values are in bold.

Table S7. Gene Ontology (GO) term analysis in the UAAAUC group

Gene WB ID	Gene public name	Sequence name (gene)	GO ID (merged)
WBGene00000160	apb-1	Y71H2B.10	GO:0008565 | GO:0002119 | GO:0000003 | GO:0040007 | GO:0030131 | GO:0006886 | GO:0009792 | GO:0005488 | GO:0030117 | GO:0006898 | GO:0006461 | GO:0016192 | GO:0005515
WBGene00000254	bli-4	K04F10.4	GO:0009790 | GO:0010171 | GO:0002119 | GO:0004289 | GO:0040007 | GO:0018996 | GO:0009792 | GO:0040002 | GO:0016808 | GO:0016021 | GO:0040011 | GO:0006508 | GO:0005634
WBGene00000383	cdc-14	C17G10.4	GO:0040010 | GO:0030496 | GO:0003676 | GO:0006470 | GO:0004725 | GO:0016791 | GO:0008138 | GO:0005819 | GO:0016311
WBGene00000397	cdh-5	F08B4.2	GO:0005509 | GO:0016020 | GO:0007156 | GO:0016021
WBGene00000415	ced-1	Y47H9C.4	GO:0005886 | GO:0005509 | GO:0005044 | GO:0043652 | GO:0016021 | GO:0043654
WBGene00001340	etr-1	T01D1.2	GO:0010171 | GO:0003723 | GO:0002119 | GO:0005576 | GO:0009792 | GO:0018991 | GO:0048477 | GO:0003676 | GO:0040011 | GO:0000166
WBGene00001518	gar-2	F47D12.1	GO:0004977 | GO:0016021 | GO:0004981 | GO:0016759 | GO:0006011 | GO:0016020 | GO:0004989 | GO:0016907 | GO:0007186 | GO:0001584
WBGene00003153	mca-3	Y67D8C.10	GO:0040010 | GO:0006810 | GO:0016021 | GO:0006812 | GO:0008152 | GO:0002119 | GO:0008340 | GO:0009792 | GO:0003824 | GO:0006897 | GO:0016020 | GO:0051481 | GO:0015085 | GO:0040011 | GO:0006816 | GO:0005388 | GO:0005886 | GO:0005509 | GO:0040017 | GO:0016820 | GO:0005524 | GO:0015662 | GO:0045807
WBGene00003154	mcm-2	Y17G7B.5	GO:0008094 | GO:0003677 | GO:0017111 | GO:0000003 | GO:0009792 | GO:0015979 | GO:0040035 | GO:0005634 | GO:0015995 | GO:0005524 | GO:0000166 | GO:0016851 | GO:0006270
WBGene00003196	mel-11	C06C3.1	GO:0040010 | GO:0019684 | GO:0006118 | GO:0005737 | GO:0000003 | GO:0009792 | GO:0045156 | GO:0005913 | GO:0030077
WBGene00003375	mlp-1	T04C9.4	GO:0008270
WBGene00003916	par-1	H39E23.1	GO:0045167 | GO:0009949 | GO:0000003 | GO:0009792 | GO:0040025 | GO:0004674 | GO:0016020 | GO:0006468 | GO:0040035 | GO:0009880 | GO:0004672 | GO:0004713 | GO:0030010 | GO:0005524 | GO:0005938
WBGene00003936	pat-12	T17H7.4	GO:0040010 | GO:0002119 | GO:0040007 | GO:0009792 | GO:0018996
WBGene00004161	pqn-80	Y111B2A.14	GO:0000003 | GO:0009792
WBGene00004373	rme-1	W06H8.1	GO:0005515 | GO:0005737 | GO:0003924 | GO:0005525 | GO:0012505 | GO:0005509 | GO:0005622 | GO:0006898
WBGene00004389	rnp-6	Y47G6A.20	GO:0040010 | GO:0004499 | GO:0042309 | GO:0050825 | GO:0002119 | GO:0000003 | GO:0009792 | GO:0050826 | GO:0018991 | GO:0050660 | GO:0050661 | GO:0003676 | GO:0040035 | GO:0040011 | GO:0000166
WBGene00004830	slo-1	Y51A2D.19	GO:0005216 | GO:0016021 | GO:0008152 | GO:0042493 | GO:0046928 | GO:0003824 | GO:0045202 | GO:0005249 | GO:0031430 | GO:0048149 | GO:0043050 | GO:0050804 | GO:0016020 | GO:0030018 | GO:0005488 | GO:0045214 | GO:0040011 | GO:0015269 | GO:0008076 | GO:0006811 | GO:0006813
WBGene00004946	sop-3	Y71F9B.10	GO:0040010 | GO:0010171 | GO:0002119
WBGene00006490	tag-144	F36H1.2	GO:0040010 | GO:0010171 | GO:0016021 | GO:0005737 | GO:0000003 | GO:0004812 | GO:0002009 | GO:0006412 | GO:0040035 | GO:0006418 | GO:0005524 | GO:0000166
WBGene00006588	tnt-3	C14F5.3	GO:0006952 | GO:0071688 | GO:0043050 | GO:0019915
WBGene00006594	tom-1	M01A10.2	GO:0002119 | GO:0040007 | GO:0009792 | GO:0031201 | GO:0016082 | GO:0040011
WBGene00006751	unc-11	C32E8.10	GO:0005543 | GO:0042309 | GO:0050825 | GO:0000003 | GO:0009792 | GO:0050826 | GO:0030276 | GO:0005545 | GO:0030118 | GO:0040011 | GO:0042734 | GO:0048488 | GO:0009791 | GO:0048268
WBGene00006759	unc-22	ZK617.1	GO:0005737 | GO:0004812 | GO:0004674 | GO:0006468 | GO:0006412 | GO:0040011 | GO:0004672 | GO:0006418 | GO:0004713 | GO:0005524 | GO:0031672 | GO:0000166
WBGene00006779	unc-43	K11E8.1	GO:0040018 | GO:0004674 | GO:0006468 | GO:0040011 | GO:0004672 | GO:0040017 | GO:0004713 | GO:0005524
WBGene00006780	unc-44	B0350.2	GO:0040010 | GO:0010171 | GO:0007165 | GO:0004553 | GO:0005515 | GO:0040018 | GO:0005975 | GO:0016328 | GO:0040011 | GO:0040017
WBGene00006791	unc-57	T04D1.3	GO:0005515 | GO:0005737 | GO:0004674 | GO:0006468 | GO:0040011 | GO:0004672 | GO:0004713 | GO:0005524 | GO:0031594

Table S7. Cont.

Gene WB ID	Gene public name	Sequence name (gene)	GO ID (merged)
WBGene00006820	unc-89	C09D1.1	GO:0005021 | GO:0005089 | GO:0005975 | GO:0004674 | GO:0035023 | GO:0006468 | GO:0040011 | GO:0004672 | GO:0004713 | GO:0005622 | GO:0005524 | GO:0031672
WBGene00008570	F08A10.1	F08A10.1	GO:0016021 | GO:0016286 | GO:0016020 | GO:0005516 | GO:0005267 | GO:0015269 | GO:0006813
WBGene00008694	F11C1.5	F11C1.5	GO:0004176 | GO:0005840 | GO:0017111 | GO:0019001 | GO:0004871 | GO:0006412 | GO:0016887 | GO:0004252 | GO:0003735 | GO:0007186 | GO:0005622 | GO:0005524 | GO:0000166 | GO:0006508
WBGene00010573	K04H4.2	K04H4.2	GO:0040010 | GO:0006030 | GO:0008061 | GO:0002119 | GO:0040007 | GO:0005576 | GO:0040011
WBGene00012543	nkcc-1	Y37A1C.1	GO:0006810 | GO:0016021 | GO:0016020 | GO:0005215 | GO:0006811
WBGene00012814	Y43F8B.3	Y43F8B.3	GO:0004867
WBGene00013011	Y48E1B.14	Y48E1B.14	GO:0016021 | GO:0007154 | GO:0005515 | GO:0000003 | GO:0004871 | GO:0007242 | GO:0035091
WBGene00013481	Y69H2.3	Y69H2.3	GO:0004857
WBGene00013805	Y116A8C.28	Y116A8C.28	GO:0004089 | GO:0015976 | GO:0008270
WBGene00015735	C13B9.4	C13B9.4	GO:0016021 | GO:0007189 | GO:0016020 | GO:0040011 | GO:0004948 | GO:0006874 | GO:0045762 | GO:0004930
WBGene00016022	C23H3.9	C23H3.9	GO:0016021 | GO:0016787
WBGene00016115	C25H3.6	C25H3.6	GO:0003677 | GO:0003702 | GO:0010171 | GO:0003746 | GO:0005515 | GO:0002119 | GO:0040007 | GO:0006355 | GO:0009792 | GO:0006354 | GO:0006350 | GO:0030528 | GO:0040011 | GO:0005634 | GO:0016068
WBGene00016197	pxl-1	C28H8.6	GO:0040010 | GO:0002119 | GO:0040007 | GO:0009792 | GO:0003676 | GO:0008270
WBGene00016561	C41D11.1	C41D11.1	GO:0000003
WBGene00017778	psf-1	F25B5.7	GO:0004872 | GO:0016021 | GO:0002119 | GO:0051260 | GO:0002009 | GO:0016020 | GO:0003676 | GO:0007155 | GO:0000166
WBGene00018794	F54C4.3	F54C4.3	GO:0040010 | GO:0002119 | GO:0000003 | GO:0040007 | GO:0009792 | GO:0002009 | GO:0003676 | GO:0040011 | GO:0008270 | GO:0005622 | GO:0040015
WBGene00019636	gsto-3	K10F12.4	GO:0005737 | GO:0008152 | GO:0015035 | GO:0045454 | GO:0004364 | GO:0009055
WBGene00021394	Y38C1AA.1	Y38C1AA.1	GO:0016021 | GO:0008152 | GO:0008415
WBGene00021562	nuo-5	Y45G12B.1	GO:0040010 | GO:0042773 | GO:0006118 | GO:0016651 | GO:0002119 | GO:0040007 | GO:0009792 | GO:0051536 | GO:0016020 | GO:0003676 | GO:0008137 | GO:0016491 | GO:0008270 | GO:0005622 | GO:0009055
WBGene00021784	cogc-4	Y51H7C.6	GO:0040010 | GO:0002119 | GO:0040007 | GO:0009792 | GO:0018991 | GO:0002009 | GO:0040035 | GO:0040011 | GO:0035262 | GO:0030334
WBGene00022500	lfi-1	ZC8.4	GO:0007165 | GO:0016032 | GO:0043565 | GO:0046983 | GO:0005828 | GO:0003700 | GO:0006355 | GO:0004871 | GO:0005634
WBGene00185002	K11H3.8	K11H3.8	GO:0005622 | GO:0008270

UAAAUC group: genes with at least two alternative splice sites, that each contains a UAAAUC element in an adjacent intron.